Heliyon 9 (2023) e20047

Contents lists available at ScienceDirect

Heliyon

journal homepage: www.cell.com/heliyon

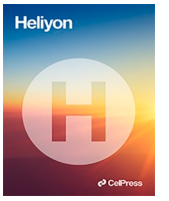

Analysis of HepG2 cell response to a wide concentration range of mitomycin C using a multichannel quartz crystal microbalance system with a microscope

Hiroshi Muramatsu *, Masahiro Naka, Sae Ito, Maki Kawamura

School of Bioscience and Biotechnology, Tokyo University of Technology, 1401-1 Katakura, Hachioji, Tokyo 192-0982, Japan

ARTICLE INFO

Keywords:
Quartz crystal microbalance
HepG2 cells
Mitomycin C
Modeling curves
Cumulative log-normal distribution
First-order lag response

ABSTRACT

The morphological response of HepG2 cells to mitomycin C was analyzed using a multichannel quartz crystal microbalance system equipped with a home-built movable microscope that enables the simultaneous acquisition of cell images and measurements of eight-channel quartz crystal microbalance. After 24 h of cell seeding, mitomycin C was injected into the culture medium. During the attachment process, the resonant frequency decreased, and the curves fitted well with the first-order lag response. Analysis of the response to mitomycin C revealed that the resonant frequency response curves varied with mitomycin C concentration. When the mitomycin C concentration was <10 μmol L^{-1}, the delay time was observed before the increase in resonant frequency. When the mitomycin C concentration was extremely low, an additional decrease in resonant frequency was observed in the middle of the delay time that fitted well with the cumulative log-normal distribution curve. The resonant frequency response curves after the delay time fitted well with the cumulative log-normal distribution curves. The delay time and mean cumulative log-normal distribution time for the increase in resonant frequency correlated with the mitomycin C concentration; however, the mean time for the additional decrease in the resonant frequency did not show a statistically significant difference as a function of mitomycin C concentration. For mitomycin C concentrations of >20 μmol L^{-1}, the response to the change in resonant frequency was rapid, and the response curves fitted well with the first-order lag response. The first-order lag response indicates that the response occurred simultaneously for all cells. The results showed that the time constant was independent of the tested mitomycin C concentration between 20 and 100 μmol L^{-1}. These results suggested that different cell death processes occurred by mitomycin C. The findings of this study suggest that the system can be used to investigate cell death in adherent cells.

1. Introduction

The quartz crystal microbalance (QCM) is a highly sensitive microbalance for detecting a change in the surface mass with changes in resonant frequency [1]. The resonant frequency of a quartz crystal changes with the mass loading of a viscous fluid that is in contact with the crystal surface. The resonant resistance is affected by the resistance of the viscous materials [2–4]. Therefore, QCM has been used for monitoring a chemical or biological phenomenon based on the resonant frequency change and resonant resistance or dumping

* Corresponding author.
E-mail address: muramatu@stf.teu.ac.jp (H. Muramatsu).

https://doi.org/10.1016/j.heliyon.2023.e20047
Received 26 October 2022; Received in revised form 8 September 2023; Accepted 8 September 2023
Available online 11 September 2023

factor [3–8]. QCM has also been used to examine the cell attachment process, focusing on the interaction between cultured cells and the surface of attached cells [9–31]. The effects of cell density [9–13] and species [14–16] on the change in the resonant frequency of a quartz crystal have been studied. Polystyrene (hydrophobic surface), metals (hydrophilic surface), and polypeptides have been used to examine the interaction between the cell surface and cultured cells [17–27]. The effects of cell growth factors, inhibitors, and toxins on cell attachment and growth processes have been investigated [28–31]. In these studies, the resonant resistance or dumping factor has been used to analyze the changes in cell characteristics [12–31].

Some studies have shown that the change in the resonant frequency of quartz crystals fits with the cell attachment model curves [9, 13,15,27]. In these studies, the cell attachment curves fitted well with the first-order lag response curves [13,27]. In this study, transparent indium-doped tin oxide (ITO) electrodes served as the electrodes of the quartz crystal, enabling the simultaneous acquisition of transparent cell images and resonant frequency measurements. With the injection of an antitumor agent, the cell response was also examined using QCM [13]. In this study, we analyzed the response of HepG2 cells to cisplatin and revealed that the change in resonant frequency response curves fitted with the cumulative log-normal distribution (CLND) curve. This indicates that the cell response follows a statistical distribution. We aimed to determine whether this response is similar to the response to other antitumor reagents by analyzing the cell response to mitomycin C (MMC).

MMC is an antibiotic and anticancer drug that mainly crosslinks deoxyribonucleic acid (DNA), leading to DNA degradation. MMC inhibits cell division and is used to regulate the cell cycle. This function is used to prepare a feeder cell layer for induced pluripotent stem cells [32–42]. Moreover, MMC induces apoptosis at a certain concentration [39]. These functions depend on the MMC concentration to treat cells. Although MMC may not be an appropriate first-line treatment due to the recent development of several antitumor medications, it has been used in the treatment of liver cancer for several years and is an important antitumor reagent for cell biology. In addition, MMC is used to prepare a feeder cell layer for culture stem cells. Several studies have been reported on MMC; however, to the best of our knowledge, there are no reports on the monitoring of continuous morphological changes using numerical values.

In this study, we constructed an eight-channel QCM system equipped with a home-built microscope that enables the monitoring of cell images in each channel. Additionally, we examined the response of HepG2 cells to a wide concentration range of MMC.

2. Materials and methods

2.1. Materials and chemicals

An AT-cut quartz crystal with a size of $8 \times 8 \times 0.18$ mm^3 and basic resonant frequency of 9.0 MHz was used with ITO electrodes. ITO electrodes were constructed using a sputtering instrument (CFS-4ES; Shibaura Mechatronics, Kanagawa, Japan) with 0.8 Pa Ar containing 5% O_2 at a radiofrequency radiation of 350 W. ITO electrodes were subjected to a 2-h heat treatment at 160 °C to stabilize the optimal oxygen ratio.

For the experiments, the HepG2 cell line (Dainippon Sumitomo Pharma, Osaka, Japan) was precultured on collagen I-coated culture plates (AGC Techno Glass, Shizuoka, Japan) For cell culture, Dulbecco's modified eagle's medium (Sigma-Aldrich) with 10%

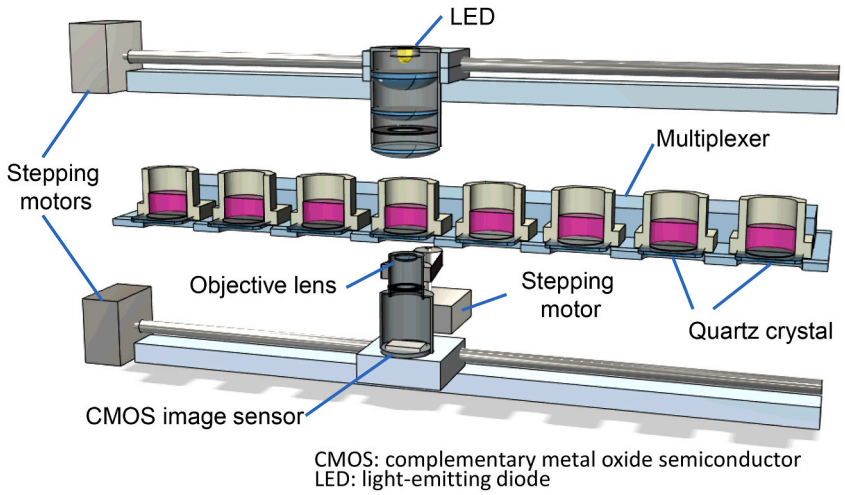

Fig. 1. Schematic diagram of the microscope and quartz crystal microbalance (QCM) system. The system consists of an eight-channel multiplier of the QCM and a moving microscope to simultaneously facilitate the measurement of eight samples: Quartz crystals with indium-doped tin oxide electrodes were placed in sample wells and positioned over a microscope equipped with a complementary metal oxide semiconductor (CMOS) image sensor. The light source unit was located above the quartz crystal to transfer the images. To acquire cell images, the microscope and light-emitting diode (LED) illumination unit were moved to each channel at a constant interval. The focus of the microscope was adjusted by rotating the object lens tube with a timing belt and stepping motor./Footnote: CMOS: complementary metal oxide semiconductor, LED: light-emitting diode, QCM: quartz crystal microbalance.

bovine serum (Biowest) and 1% antibiotic antimycotic (Sigma-Aldrich) was used.

Cells were trypsinized with trypsin–ethylenediaminetetraacetic acid (0.5%, 10 ×) (Gibco). Further, 0.01% poly-L-lysine (PLL) (molecular weight, 150,000–300,000) solution (Sigma-Aldrich) was used for preparing the extracellular matrix on the quartz crystal. MMC (1 mg mL^{-1}) and ethylene glycol were obtained from Fujifilm Wako Pure Chemical Industries (Osaka, Japan). Ethanol was obtained from Sigma-Aldrich. Lactate dehydrogenase assay kit was obtained from Dojindo Laboratories (Kumamoto, Japan).

2.2. Experimental instruments

In our study, we used an eight-channel quartz crystal microbalance (QCM) measuring system comprising a QCM unit (QCM922A) and eight-channel multiplexer (QCM922A-900) obtained from Seiko EG&G. QCM 922A measures the admittance of the quartz crystal around the resonant frequency via an AC sweep analysis using the four-terminal method. Accordingly, it searches and calculates the resonant frequency of the quartz crystal. The multiplier switches the wires to connect the selected channel of the quartz crystal with the relay circuits. The QCM unit and multiplier were supplied together from the manufacturer and tested by the manufacturer beforehand.

We constructed an eight-channel measuring system that can simultaneously measure QCM parameters and obtain photographic images in a CO_2 incubator. The microscope–QCM system was constructed using the eight-channel QCM multiplier and a home-built microscope unit that moves to each QCM channel via a stepping motor mechanism. Fig. 1 depicts a schematic of a microscope paired with QCM. Quartz crystals with ITO electrodes were placed in sample wells and positioned over a microscope equipped with a complementary metal oxide semiconductor (CMOS) image sensor. The light-emitting diode (LED) illumination unit was located above the quartz crystal to transfer the images. To acquire cell images, the microscope and light source unit were moved to each channel at a constant interval. The focus of the microscope was adjusted by rotating the object lens tube with a timing belt and stepping motor. The working unit was used inside the CO_2 incubator (model E−50, AsOne, Osaka, Japan).

Fig. S1a shows a photograph of the working unit. The unit is constructed on an aluminum frame with the multiplexer unit, the microscope unit and the illumination unit. The microscope unit and the illumination unit were on the rails to move to each channel by stepping motors and timing belts. The quartz crystals in the sample wells are connected to the multiplexer unit, and the sample wells are attached to a sample stage with fastening components. Fig. S1b shows a photograph of the microscope unit. The microscope unit is located beneath the sample stage and comprises the objective lens, the CMOS image sensor, and two stepping motors: one for focus control through a timing belt and another for depth positioning. Most of the plastic components in these units were made using a 3D printer.

The video signal from the CMOS image sensor was transmitted to a personal computer (PC) via a Universal Serial Bus (USB) interface. The stepping motors were used to move the microscope and light source unit as well as to adjust the focus of the microscope. The stepping motors and power lines for the light source were controlled using a driver board (Lamps 1.6) and microcomputer board (Arduino MEGA 2560) with a USB connection to a PC. The resonant frequency and resistance of up to eight quartz crystals were monitored every 10 s using QCM922A through a multiplier unit. Microscopy images for each channel were automatically stored every 30 min in the PC. In this study, a four-channel type measuring system was also used as described previously [13].

2.3. Experimental Procedure

To prepare test cells, the quartz crystal was sandwiched with silicone O-rings and attached to a well-type cell made of polyether ether ketone (model QA-CL5PK-A, Seiko EG&G, Tokyo, Japan). The quartz crystal was connected to the multiplexer in the CO_2 incubator and fixed to the instrument with fixing parts, then the monitoring of the resonant frequency and resonant resistance was started. The ITO electrode on the quartz crystal was treated with PLL solution (0.01%, 50 μL) for 2 h and then rinsed with a culture medium. Next, 200 μL of the culture medium was added to each well. After injecting the culture medium, we waited for 2 h so that the quartz crystal stabilized. Before seeding, HepG2 cells were the trypsinized and centrifuged. The centrifuged cells were suspended in the culture medium, and the cell concentration was measured with a hemocytometer to prepare the cell suspension for each well. Cell densities of 300–600 cells mm^{-2} were used to obtain an effective quartz crystal surface area (inner diameter of 5.5 mm), which corresponded to a seeded cell number of 7000–14000 cells per well. After seeding the cell, a cap with a glass window was placed on the top of the well, and microscope monitoring was started promptly. The MMC solution was diluted to 1:10–1:50 if necessary. After 24 h of cell seeding, approximately 2–40 μL of the solution was injected to adjust the final MMC concentration to be between 0.1 and 100 μmol L^{-1}. Measurements within the range of MMC concentration of 2–20 μmol L^{-1} were replicated two or three times because this range is critical for cell response. A series of single measurements were conducted to investigate the dose response of MMC for other concentration ranges.

2.4. Statistical analysis

The relationship between MMC concentration and the obtained parameter in this study was analyzed using the regression analysis. The slope of the regression line was obtained using the least-squares method and was tested under the statistical hypothesis that it equals zero. The total variance and the variance of the slope factor were compared using the t-distribution curve and the p-value obtained for the case to check for statistically significant differences. The p-value of 0.05 was used to check for statistically significant differences since a 95% confidence level was used for the statistical decision in this study.

3. Results and discussion

3.1. Response curve for cell attachment and mitomycin C injection

Fig. 2 shows the typical change in resonant frequency and resistance in this study. To facilitate easier identification of the difference and trends, the resonant frequency and resistance were replotted in each group by normalizing the amplitude of cell attachment after 24 h from the cell seeding (Fig. S2). Fig. S2a shows the resonant frequency responses and Fig. S2b shows the resonant resistance responses.

Fig. 2a shows the typical resonant frequency response for the cell attachment and growth processes without using MMC. The resonant frequency rapidly decreased immediately after cell seeding. As the resonant frequency change occurred according to the change in the mass of the vibrating quartz crystal, cell spreading and flattening of the quartz crystal surface increased the vibration mass and altered the resonant frequency. Fig. S3a presents the simultaneous acquisition of microscopy images at 0.5, 24, 48, and 96 h after cell seeding. At 0.5 h, trypsinized cells were round in shape. Cells spread at 24 h, grew at 48 h, and finally achieved confluency at 96 h after seeding.

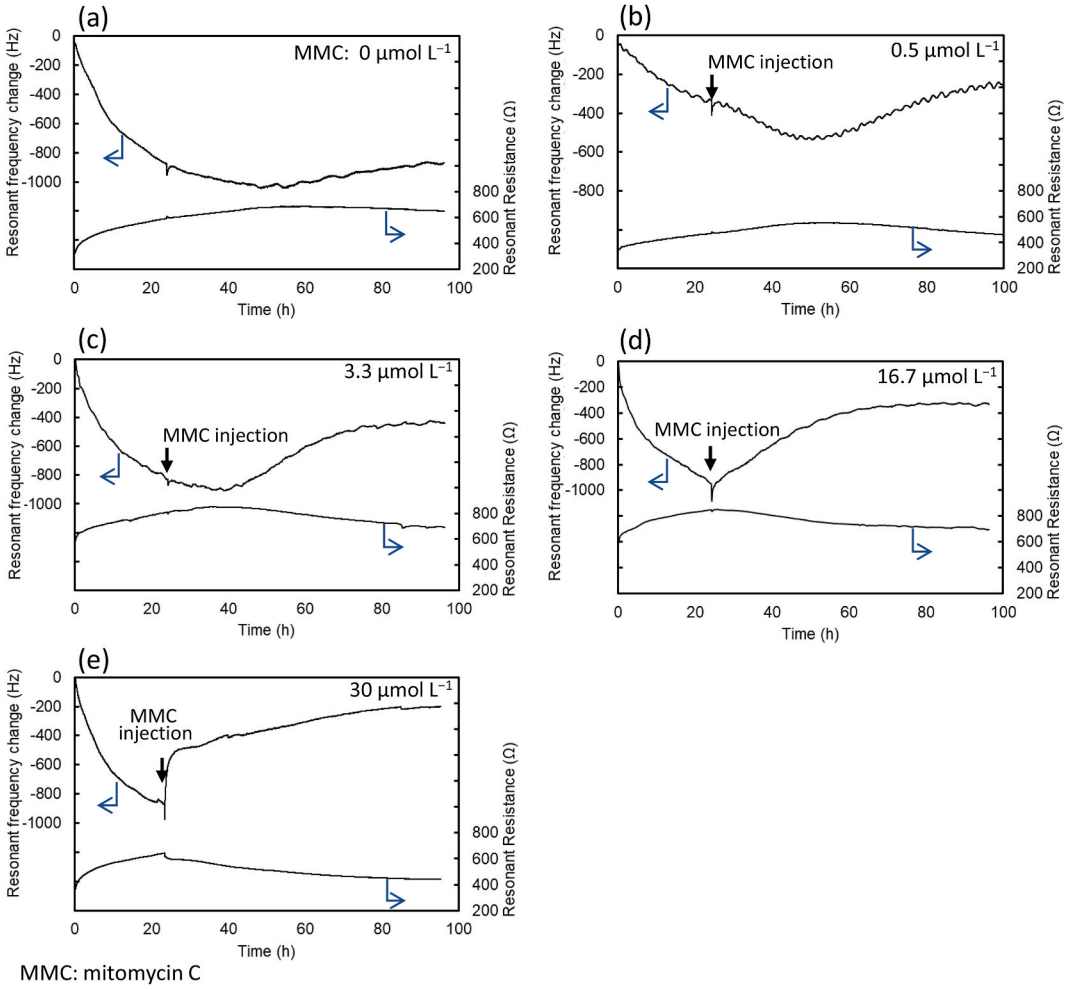

Fig. 2. Typical resonant frequency and resistance response curves for cell attachment and response processes with and without mitomycin C (MMC): (a) without MMC and (b) 0.5, (c) 3.3, (d) 16.7, and (e) 30 µmol L^{-1} MMC injected at 24 h: **(a)** The resonant frequency rapidly decreased immediately after cell seeding. The cell spreading and flattening of the quartz crystal surface altered the resonant frequency. The cell-cell contact increases the resonant frequency by reducing the cell contact area and the strength of interaction with the plate. **(b)** The resonant frequency continued to decrease after MMC injection, and began to decrease even more approximately 8 h after MMC injection. After 24 h of MMC injection, the resonant frequency increased. **(c)** The increase of resonant frequency delayed for 10 h from MMC injection. The delay time was shorter than the response for 0.5 µmol L^{-1} MMC injection, and no additional decrease in resonant frequency was observed during the delay time. The plural experimental data revealed that the delay time was shortened due to increased MMC concentration. **(d)** The resonant frequency increased gradually following the MMC injection and no delay time was observed for the resonant frequency increase after the MMC injection. **(e)** The resonant frequency response following the MMC injection was rapid, and no delay time was observed./Footnote: MMC: mitomycin C.

Fig. 3a illustrates the cell attachment and growth processes. As shown in the figure, the sphere cells fall and attach to the quartz crystal surface (P1), which increases the mass; cells spread and attach to the surface (P2), which also increases the mass; and cells multiply to form clusters (P3), and the cell–cell interaction increases the cell height and decreases the contact area.

The resonant frequency decreases in the cell attachment and multiplication process. In contrast, the cell–cell contact increases the resonant frequency as it induces a decrease in the cell contact area on the plate and the strength of cell contact with the plate [13,15]. As the resonant frequency reflects the mass loading of rigid and viscous materials on the quartz crystal, whereas the resonant resistance reflects only the vibration energy loss on the quartz crystal surface, the resonant frequency and resistance were plotted in Fig. S4a. The resonant resistance–resonant frequency curves were essentially linear; however, the ratio of resonate resistance to resonant frequency increased slightly during the first attachment and subsequent processes during the cell–cell contact. This indicates that cell viscosity increases during the processes of cell attachment and cell–cell contact.

Fig. 2b shows the response curves of resonant frequency and resistance for the injection of 0.5 μmol L^{-1} MMC 24 h after cell seeding. As shown in the figure, the resonant frequency continued to decrease after MMC injection, and the attachment process persisted. Furthermore, the resonant frequency began to decrease approximately 8 h after MMC injection. After 24 h of MMC injection, the resonant frequency increased. Cell images are shown in Fig. S3b. The cells were round in shape at 0.5 h and attached to the surface at 24 h. The cells became flat at 48 h and partly long and rounded narrow in shape at 92 h. It was noted that cell division ceased after MMC injection.

An additional decrease in resonant frequency was observed after 8 h of MMC injection (Fig. 2b). A decrease in resonant frequency

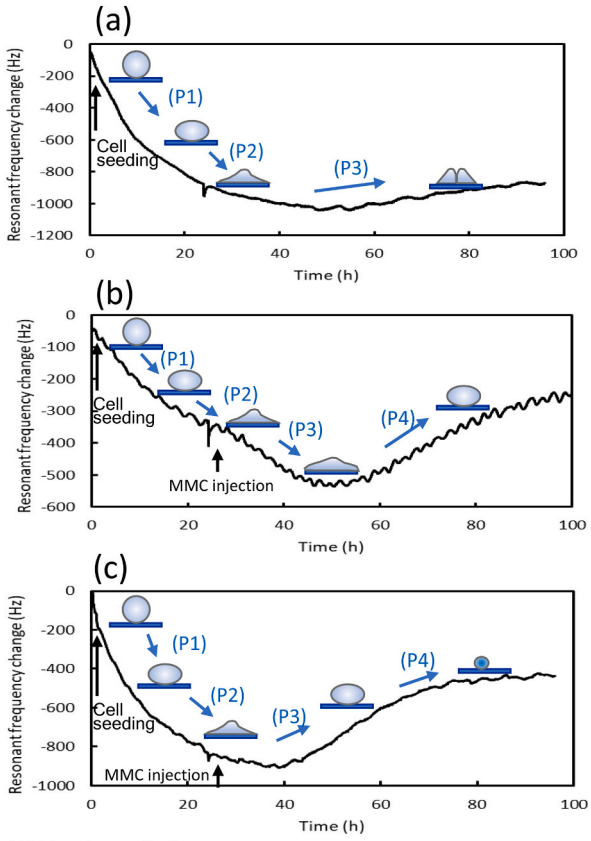

MMC: mitomycin C

Fig. 3. Illustration of the morphological changes in cells during the attachment process and response to mitomycin C (MMC). These illustrations represent the cell attachment and growth process without MMC (a), cell attachment and response to very low-concentration MMC (b), and cell attachment and response to medium- and high-concentration MMC (c): **(a)** The following three steps illustrate the process of cell attachment and growth: (P1) the sphere cells fall and attach to the quartz crystal surface, which increases the mass; (P2) cells spread and attach to the surface, which also increases the mass; and (P3) cells multiply to form clusters, and the cell–cell interaction increases the cell height and decreases the contact area. **(b)** The following four steps illustrate the process for low-concentration MMC: (P1) the sphere cells fall and attach to the quartz crystal surface, increasing the mass; (P2) cells spread and attach to the surface, which also increases the mass; (P3) cells are in close contact with the surface as the first response to MMC, which increases the mass; and (P4) the cells become rounded in shape as seen in the cell images of Fig. S3b, indicating a weakened cellular attachment strength and a consequent decrease in the mass factor. **(c)** The following four steps illustrate the process for medium- and high-concentration MMC: (P1) the sphere cells fall and attach to the quartz crystal surface, increasing the mass; (P2) the cells spread and attach to the surface, which also increases the mass; (P3) as the strength of the cell attachment weakens, the cells become round in shape, which decreases the mass; and (P4) cell shrinking decreases the mass during the cell death process./Footnote: MMC: mitomycin C.

may occur when the interaction between the quartz crystal surface and cells increases. A possible reason is the loss of microvilli from the cell surface,[37] which facilitates close contact between the cells and quartz crystal surface. After 24 h of MMC injection, the resonant frequency increased. The increase in the resonant frequency can be interpreted from the microscopy images as the contacting area of the cells decreased when the cells became round in shape.

Fig. 3b illustrates cell attachment and the response to MMC injection. As shown in the figure, the sphere cells fall and attach to the quartz crystal surface, increasing the mass (P1); cells spread and attach to the surface, which also increases the mass (P2); cells are in close contact with the surface as the first response to MMC (P3), which increases the mass; and the cells become rounded in shape (P4) as seen in the cell images of Fig. S3b, indicating a weakened cellular attachment strength and a consequent decrease in the mass factor.

A small drift in the resonant frequency was observed, as depicted in Fig. 2b. It is supposed that the drift was induced by varying of the frequency scan range of admittance measurement in QCM922A. The calculated results of the QCM resonant frequency includes a certain error that may be affected when the scan range is changed. As the scan range is decided automatically related to the resonant resistance amplitude in QCM922A, the scan range varies frequently if the condition changed around the border line to change the scan range. Consequently, the small drift in the calculated resonant frequency is observed. The crucial point is that the drift is observed only in the range of the calculation error, and the resonant frequency is obtained in the range of the error. In the experiments, the resonant frequency variation caused by the cell response is much larger than the drift of the resonant frequency. Therefore, the data can be used as the response of the cultured cells.

Fig. 2c shows the responses of resonant frequency and resistance for 3.3 μmol L^{-1} MMC injection. The delay time from MMC injection until the increase in resonant frequency was 10 h, which was shorter than the response for 0.5 μmol L^{-1} MMC injection, and no additional decrease in resonant frequency was observed during the delay time. The plural experimental data revealed that the delay time was shortened due to increased MMC concentration, as described later. Cell images are shown in Fig. S3c. The cells were round in shape at 0.5 h and spread at 24 h. Some cells became small and round at 48 h, and partly shrunken cells were observed at 96 h. This result showed that cell division ceased after MMC injection and the cells were partly dead at 96 h.

Fig. 3c illustrates cell attachment and response to MMC injection. As shown in the figure, the sphere cells fall and attach to the quartz crystal surface (P1), increasing the mass; the cells spread and attach to the surface (P2), which also increases the mass; as the strength of the cell attachment weakens, the cells become round in shape (P3), which decreases the mass; and cell shrinking (P4) decreases the mass during the cell death process.

The resonant frequency and resistance response for 16.7 μmol L^{-1} MMC injection are depicted in Fig. 2d. In this case, no delay time was observed, and the resonant frequency increased gradually following the MMC injection. Cell images are displayed in Fig. S3d. The cells were round at 0.5 h and spread at 24 h. At 48 h, most cells shrank and formed small particles, and they further shrank at 96 h. Although the timing was different, the morphological change was similar to that shown in Fig. 3c.

Fig. 2e shows the resonant frequency and resistance response for 30 μmol L^{-1} MMC injection. Notably, this response was rapid, and no delay time was observed. Cell images are shown in Fig. S3e. The cells were round at 0.5 h and spread at 24 h. The cells became round and small at 48 h and further shrank at 96 h. The changes in cell morphology after 30 μmol L^{-1} MMC injection were slower than those after 16.7 μmol L^{-1} MMC injection. This result indicated that the high-concentration MMC function was too strong to respond the cells as the morphology change. In this case, the morphological change is similar to that shown in Fig. 3c, although the resonant frequency response curves appeared vastly different.

To verify the relationship between resonant frequency and resistance, the resonant frequency and resistance (F–R) diagram was plotted (Figs. S4a, S4b, S4c, S4d, and S4e). The F–R diagram reveals the elements that cause the change in the resonant frequency. The resonant frequency changes due to both mass and viscosity factors, while the resonant resistance shows only changes based on the viscosity factor. Attaching a rigid material to the quartz crystal leads to a decrease in the resonant frequency without an increase in the resonant resistance. When the quartz crystal contacts with a viscous material, the resonant frequency decreases and the resonant resistance increases.

The F–R diagram without MMC injection is shown in Fig. S4a. Fig. S4a shows that cell seeding decreased the resonant frequency and increased the resonant resistance. The slope of the F–R diagram was slightly steep in the initial step of part A, gentle in the next part B and slightly steep again in part C. This suggests that the viscosity was slightly higher in the initial cell attachment step (part A) and dense cell step (part C) compared to cell elongation step (part B). In the last step of part D, the resonant frequency increased when the cells were over confluent but the resonant resistance remained high. The increase in resonant frequency suggests a decrease in the rigid element at the cell-quartz crystal interface. However, the high resonant resistance level suggests that the viscos element was still increasing in this step.

Figs. S4b, S4c, S4d, and S4e represent the diagrams for the four concentrations (0.5, 3.3, 16.7 and 30 μmol L^{-1}) of MMC injection. The F–R curves in these figures are similar to that in Fig. S4a during the cell attachment process. In Figs. S4b, S4c, and S4d, the resonant frequency decreased in part E after MMC injection, indicating a reduction in the cell adhesion area in this part. In contrast, the resonant resistance in part E was higher than in the cell adhesion step. This implies that the cell viscosity after the MMC injection was higher than that during the cell adhesion step.

In Figs. S4c and S4d, the cells shrank in the last step in part F. Consequently, the resonant resistance quickly decreased in this step, and the F–R ratio returned to the initial ratio. This suggests a decrease in cell viscosity during the shrinking step.

The F–R diagram in Fig. S4e shows a similar pattern to Figs. S4c and S4c, but it is rectilinear and clear. In Fig. S4e, the resonant frequency increases in part G after MMC injection, but the decrease in resonant resistance was small in Fig. S4e. This suggests that the cells have lost their rigidity in this step, inducing an increase in cell viscosity. During the shrink process of part H, the resonant resistance decreased rapidly and the F–R ratio returned to the level of the cell attachment process. This suggests that the viscosity of cells has clearly decreased in the shrink process. Therefore, the F–R diagram presented a two-step response that occurred for middle

and high-concentration MMC.

3.2. Response patterns after MMC injection

Based on Fig. 2, S2 and S3, the response patterns of the resonant frequency change after MMC injection are divided and characterized as a delay in response (A), additional decrease in the resonant frequency change (B), gradual increase in the resonant frequency (C), and rapid increase in the resonant frequency (D).

The response for 0.5 μmol L^{-1} MMC injection (Fig. 2b) included the delay in response (A), additional decrease during the delay time (B), and gradual increase during the delay time (C). The response for 3.3 μmol L^{-1} MMC injection (Fig. 2c) included the delay response (A) and the gradual increase (C). The response for 16.7 μmol L^{-1} MMC injection (Fig. 2d) included the gradual increase (C). The response for 30 μmol L^{-1} MMC injection (Fig. 2e) included the rapid increase (D) and gradual increase (C).

The delay in response occurred for the low-concentration MMC experiments. Fig. 4 shows the correlation between the delay time and MMC concentration. The delay time decreased with increasing MMC concentration and became zero for approximately 10 μmol L^{-1} MMC. The regression curve showed that the delay time was expressed as follows: $T_{\text{delay time}}$ [h] $= -6.3 \ln(C_{\text{MMC}}) + 21.9$, where C_{MMC} is the injected MMC concentration (μmol L^{-1}). The regression analysis on the slope yielded a p-value of $7.9 \cdot 10^{-8}$ ($n = 16$), which is significantly smaller than 0.05, indicating statistical significance. This suggests that the delay time of the response curve is dependent on the MMC concentration.

The results of the lactate dehydrogenase assay 24 h after MMC injection showed that the cell membrane permeability was destroyed in most cells injected with 10 μmol L^{-1} MMC. This concentration corresponded to the concentration that disappeared during the delay time. Therefore, cells treated with 0.5 and 3.3 μmol L^{-1} MMC were still developing, and those treated with 16.7 and 30 μmol L^{-1} MMC were almost dead 24 h after MMC injection. This showed that the response to increasing resonant frequency reflects the cell death process.

3.3. Fitting the modeling curves with the resonant frequency responses

As described previously, the components of the resonant frequency response for MMC injection were organized. The response consisted of the cell attachment process and response to MMC. The components can be expressed using model equations, and the dependence of MMC concentration can be analyzed using the parameters of the model equation.

The response curve of the resonant frequency in the attachment process was primarily expressed using the first-order lag response for a cell mass loading (Eq. (1)) and cell multiplication response (Eq. (2)). The total resonant frequency response (Eq. (3)) was expressed by a multiplate of the cell mass loading, cell density, and additional effect expressed by the function $g(t)$. The function $g(t)$ included the effect of cell–cell interaction for the high-density condition. The cell density function was previously reported [13], where cell–cell contact leads to clustering of cells, weakening of the cell cluster, and decrease in the viscous mass loading around the cells. This effect was demonstrated by the cell density and probability of cell–cell contact. Furthermore, the first cell attachment to the quartz crystal surface, typically 20% of the mass load, occurred in the model. This attachment process occurred with a log-normal distribution in a few hours:

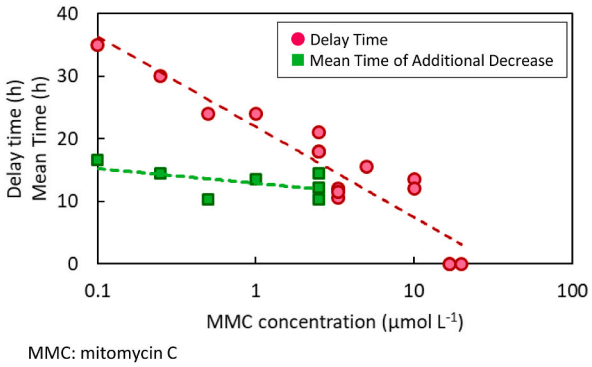

Fig. 4. Correlation between delay time and mitomycin C (MMC) concentration (●), and correlation between the mean time of the additional decrease and MMC concentration (■) in the resonant frequency responses: The delay time decreased with increasing MMC concentration and became zero for approximately 10 μmol L^{-1} MMC. The regression curve showed that the delay time was expressed as follows: $T_{\text{delay time}}$ [h] $= -6.3 \ln(C_{\text{MMC}}) + 21.9$, where C_{MMC} is the injected MMC concentration (μmol L^{-1}). The regression analysis on the slope yielded a p-value of $7.9 \cdot 10^{-8}$ ($n = 16$), which is significantly smaller than 0.05, indicating statistical significance. This indicates that the delay time of the response curve is dependent on the MMC concentration. Meanwhile, the actual mean time of the additional decrease appeared to be slightly dependent on MMC concentration and reached a plateau at approximately 5 μmol L^{-1} MMC in the delay time correlation curve. This indicated that the additional cell attachment was engulfed by decrease the contact area of cells when the MMC concentration was >5 μmol L^{-1}. The regression analysis for the slope resulted in a p-value of 0.188 ($n = 7$), indicating no statistical significance as it is greater than 0.05. This suggests that the effect of MMC concentration is uncertain in relation to the additional decrease mean time of the response curve./Footnote: MMC: mitomycin C.

$$\Delta m(\mathrm{t}) = \Delta m(\infty)\left(1 - e^{-\frac{t}{T_1}}\right) \tag{1}$$

$$n(t) = n(0) \cdot 2^{\frac{t}{T_2}} \tag{2}$$

$$\Delta F(t) = -K \cdot n(t) \cdot \Delta m(t) \cdot g(t) \tag{3}$$

where T_1 is the lag time constant, $n(0)$ is the initial cell density, t is time, T_2 is the cell doubling time, K is a factor for converting the mass loading to resonant frequency, and $g(t)$ is the response function.

The resonant frequency response curve for 0.5 μmol L^{-1} MMC injection (Fig. 2b) was constructed using the components of the delay response (A), additional attachment (B), and morphological changes to decrease the contact area (C) based on the cell attachment curve. We found that CLND can express components (B) and (C). Fig. 5a depicts the modeling curve and component curves (dashed

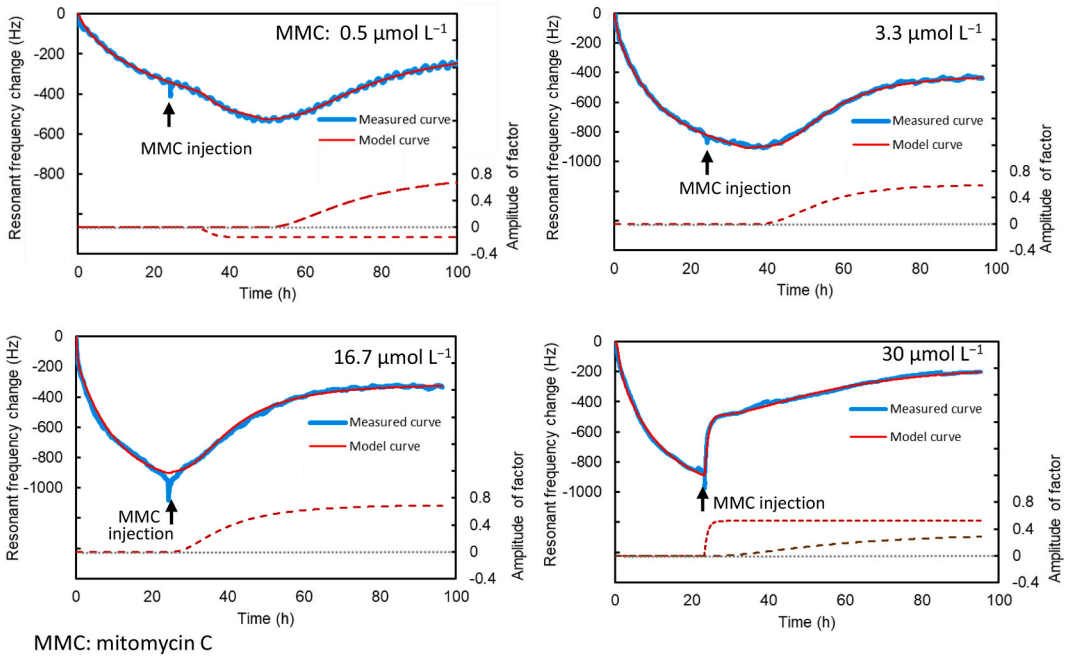

Fig. 5. Modeling curves and each component curve (dashed lines) for the resonant frequency responses. Curves in Fig. 2b–e indicate (a) 0.5, (b) 3.3, (c) 16.7, and (d) 30 μmol L^{-1} mitomycin C (MMC) injection: The response curve of the resonant frequency in the attachment process was primarily expressed using the first-order lag response for a cell mass loading $\Delta m(\mathrm{t}) = \Delta m(\infty)\left(1 - e^{-\frac{t}{T_1}}\right)$ and cell multiplication response $n(t) = n(0) \cdot 2^{\frac{t}{T_2}}$. The total resonant frequency response $\Delta F(t) = -K \cdot n(t) \cdot \Delta m(t) \cdot g(t)$ was expressed by a multiplate of the cell mass loading, cell density, and additional effect expressed by the function $g(t)$. In these equations, T_1 is the lag time constant, $n(0)$ is the initial cell density, t is time, T_2 is the cell doubling time, K is a factor for converting the mass loading to resonant frequency. The function $g(t)$ included the effect of cell–cell interaction for the high-density condition where cell–cell contact leads to clustering of cells, weakening of the cell cluster, and decrease in the viscous mass loading around the cells. Furthermore, the first cell attachment to the quartz crystal surface, typically 20% of the mass load, occurred in the model. This attachment process occurred with a log-normal distribution in a few hours. (a) For the response to 0.5 μmol L^{-1} MMC injection, the modeling curve was constructed using the components of the delay response (A), additional attachment (B), and morphological changes to decrease the contact area (C) based on the cell attachment curve. We found that the cumulative log-normal distribution (CLND) curve can express components (B) and (C). The base curve represents the cell attachment process, where cell division ceased after a 24-h delay because of MMC injection. The actual mean time of the CNLD curve could be calculated using the following formula $t_m = e^{\ln \mu + (\ln \sigma)^2/2}$ where, ln μ and ln σ indicate the mean and standard deviation of the CLND curve. For 0.5 μmol L^{-1} MMC injection, the delay time was 24 h. The actual mean time of the additional attachment was 10 h, calculated from the mean time of ln(10) h and the standard deviation of ln(1.25) h. The actual mean time of the component C was 34 h, calculated from the mean time of ln(25) h and standard deviation of ln(2.2) h. **(b)**For the response to 3.3 μmol L^{-1} MMC injection, no additional decrease in the resonant frequency was observed; however, a delay response and gradual increase in the resonant frequency were observed. A part of the resonant frequency increase could fit with the CLND curve. The mean CLND time was ln(19) h, and the standard deviation was ln(1.8) h. The actual mean time was 26 h. (c) For the response to 16.7 μmol L^{-1} MMC injection, no delay time was observed before the increase in the resonant frequency in the response curve. The rising portion of the resonant frequency curve could fit with the CLND curve. The mean CLND time was ln(15) h, and the standard deviation was ln(2.1) h. The actual mean time was 20 h. (d) For the response to 30 μmol L^{-1} MMC injection, the response was rapid, and this part of the response curve can fit with the first-order lag response. This indicated that the response occurs simultaneously for most cells. The response continued to increase gradually, which was fitted with the CLND curves. The time constant of the first-order lag response was 2.0 h, whereas the mean time of the CLND response was ln(23) h, with a standard deviation of ln(2.2) h./Footnote: CLND: cumulative log-normal distribution, MMC: mitomycin C.

lines). In Fig. 5a, the base curve represents the cell attachment process, where cell division ceased after a 24-h delay. Component B was the CLND curve with the mean time of ln(10) h and standard deviation of ln(1.25) h. Component C was the CLND curve with the mean time of ln(25) h and standard deviation of ln(2.2) h. The actual mean time of the CNLD curve could be calculated using the following formula:

$$t_m = e^{\ln \mu + (\ln \sigma)^2/2}$$

where, ln μ and ln σ indicate the mean and standard deviation of the CLND curve. For Fig. 2b, the mean times of components B and C were 10 and 34 h, respectively.

The additional decrease in the resonant frequency response occurs when the MMC concentration is extremely low. The actual mean time of the additional decrease (component B) was plotted for the observed cases (Fig. 4). The mean time appeared to be slightly dependent on MMC concentration and reached a plateau at approximately 5 μmol L^{-1} MMC in the delay time correlation curve. This indicated that component B was engulfed by component C when the MMC concentration was >5 μmol L^{-1}. The regression analysis of the slope resulted in a p-value of 0.188 (n = 7), indicating no statistical significance as it is greater than 0.05. This suggests uncertain effects of MMC concentration in relation to the mean time of the additional decrease.

In the response curve for 3.3 μmol L^{-1} MMC injection (Fig. 2c), no additional decrease in the resonant frequency was observed; however, a delay response and gradual increase in the resonant frequency were observed. A part of the resonant frequency increase could fit with the CLND curve. Fig. 5b presents the fitting curve. The mean CLND time was ln(19) h, and the standard deviation was ln (1.8) h. The actual mean time was 26 h.

No delay time was observed before the increase in the resonant frequency in the response curve for 16.7 μmol L^{-1} MMC injection (Fig. 2d). The rising portion of the resonant frequency curve could fit with the CLND curve. Fig. 5c depicts the fitting curve, where the mean CLND time was ln(15) h, with a standard deviation of ln(2.1) h. The actual mean time was 20 h.

Fig. 6a shows the correlation between the actual mean time of the CLND curves and applied MMC concentration based on 16 measurements. The regression curve of the mean time was expressed as follows: T_{mean} [h] = −5.6 ln(C_{MMC}) + 31.0. The slope regression analysis yielded a p-value of $2.3{\cdot}10^{-6}$ ($n = 16$), which is significantly smaller than 0.05, indicating statistical significance.

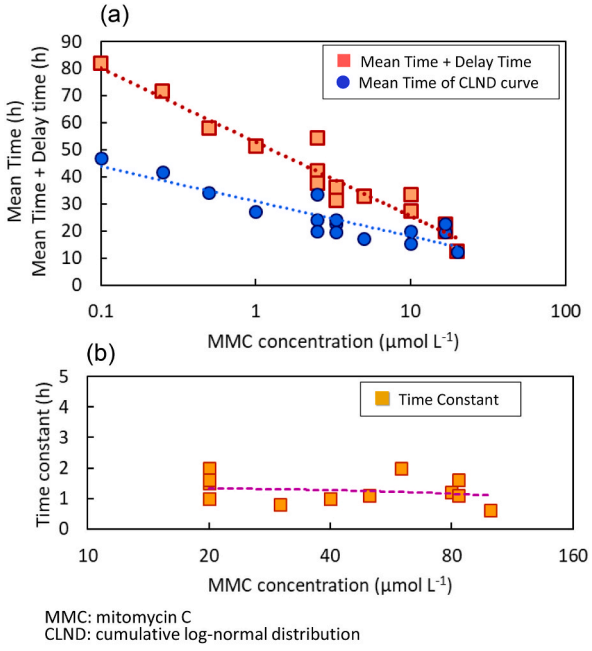

Fig. 6. (a) Correlation between the actual mean time of the cumulative log-normal distribution (CLND) curves and the concentration of mitomycin C (MMC) (●), and correlation between the sum of the delay time and the mean time of the CLND curves and applied MMC concentration (■): The regression curve of the mean time was expressed as follows: T_{mean} [h] = −5.6 ln(C_{MMC}) + 31.0. The slope regression analysis yielded a p-value of $2.3{\cdot}10^{-6}$ ($n = 16$), which is significantly smaller than 0.05, indicating statistical significance. This suggests that the actual mean time in response curve is dependent on the concentration of MMC. The sum of the delay time and the mean time of the CLND curves is the total mean response time for MMC injection. The regression curve of the total mean response time was expressed as follows: $T_{total\ response}$ [h] = −11. 9 ln(C_{MMC}) + 52.9. The slope regression analysis yielded a p-value was $2.3{\cdot}10^{-9}$ ($n = 16$), which is significantly smaller than 0.05, indicating statistical significance. This suggests that the total mean response time of the response curve is dependent on the MMC concentration. **(b)** Correlation between the time constant of the first-order lag response and the MMC concentration: For measurements with 20–100 μmol L^{-1} MMC, the response curve can fit with the first-order lag response. The time constant of the first-order lag response was 0.8–2 h, which does not depend on the MMC concentration since the p-value of the regression analysis for the slope was 0.894 ($n = 13$), which indicates there is no statistical significance as it is greater than 0.05./Footnote: CLND: cumulative log-normal distribution, MMC: mitomycin C.

This suggests that the actual mean time in the response curve relies on the concentration of MMC.

Fig. 6a also shows the correlation between the sum of the delay time and mean time of the CLND curves and applied MMC concentration. This is the total mean response time for MMC injection. According to the regression curve, the total mean response time was expressed as follows: $T_{\text{total response}}$ [h] $= -11.9 \ln(C_{\text{MMC}}) + 52.9$. The slope regression analysis yielded a p-value was $2.3 \cdot 10^{-9}$ ($n = 16$), which is significantly smaller than 0.05, indicating statistical significance. This suggests that the total mean response time of the response curve is dependent on the MMC concentration. It was evident that higher MMC concentrations led to a shorter delay time, and the mean time correlated with the logarithmic MMC concentration.

The response for 30 μmol L^{-1} MMC injection was rapid, and this part of the response curve can fit with the first-order lag response. This indicated that the response occurs simultaneously for most cells. These results showed that the response for MMC injection changes the CLND curves to the first-order lag response at a concentration of 10–20 μmol L^{-1}. The response continued to increase gradually, which was fitted with the CLND curves. The fitting curve is shown in Fig. 5d. Additionally, the time constant of the first-order lag response was 2.0 h, whereas the mean time of the CLND response was ln(23) h, with a standard deviation of ln(2.2) h. As the response pattern of the resonant frequency changed at a concentration of approximately 20 μmol L^{-1} MMC, conditions of >20 μmol L^{-1} MMC were tested up to 100 μmol L^{-1} MMC. For measurements with 20–100 μmol L^{-1} MMC, the time constant of the first-order lag response of MMC was 0.8–2 h. These time constant values are plotted in Fig. 6b. The plot is not affected by MMC concentration because the p-value of regression analysis for the slope was 0.894 (n = 13), which indicates there is no statistical significance as it is greater than 0.05. It was evident that low-concentration MMC induces the CLND response, which is a probability-dependent phenomenon, but high-concentration MMC induces the first-order delay response, as a simultaneous response of all cells.

In case of 16.7 μmol L^{-1} MMC injection, the resonant frequency gradually changed (Fig. 2d), but the shrinkage process was rapid, as shown in the 48-h image (Fig. S3d). This change indicates that the cell death process is apoptosis, as MMC is known to induce apoptosis.[39] In case of 30 μmol L^{-1} MMC injection, the resonant frequency changed rapidly (Fig. 2e), but the 48-h cell image showed no rapid change (Fig. S3e). As shown in the 96-h image (Fig. S3e), the cells started to shrink, suggesting that the cell death process is apoptosis. Thus, the experimental results suggested that high-concentration MMC induced simultaneous cell response but delayed apoptosis due to significant damage.

The fitting parameters for Fig. 5 are listed in Table S1. The decision factors were better than 0.999.

For quartz crystal measurement, the appropriate cell density range is approximately 300–1000 cells mm^{-2}. When the cell density is extremely low, the resonant frequency change will be small, making it difficult to analyze the response; however, when the cell density is extremely high, cells form clusters that weaken the cell attachment and affect the appropriate cell response measurement. Further, the application of this method is limited to adherent cells.

The effect of different types of plates for preculturing requires further confirmation. We previously tested collagen and poly-L-lysin on the quartz crystal surface [27]. The attachment of cells to the collagen surface was slower than that to the poly-L-lysin surface. In addition, although the cell response to MMC using collagen has not been tested, it may show a difference in response time.

The MMC stock solution (1 mg mL^{-1}) comprised 90 v/v% ethylene glycol and 10 v/v% ethanol. The diluted 100 μmol L^{-1} MMC contained 3.4 wt% ethylene glycol and 0.27 wt% ethanol. In case of 30 μmol L^{-1} MMC, the concentration of ethylene glycol was 1.0 wt %. As ethylene glycol is used to freeze cell stock and has weak toxicity, it is unlikely that changes in the ethylene glycol concentration lead to drastic changes in the cell response. In case of 30 μmol L^{-1} MMC, the ethanol concentration was 0.08 wt%. It is also unlikely that changes in ethanol concentration in this range lead to drastic changes in the cell response. To confirm this, a culture test was performed by adding 3.4 wt% ethylene glycol and 0.27 wt% ethanol 24 h after cell seeding. Fig. 5Sa shows microscope images of HepG2 cells with ethylene glycol and ethanol, while Fig. 5Sb shows images without the presence of ethylene glycol and ethanol. Noticeable changes were not observed in HepG2 cells after the addition of ethylene glycol and ethanol, unlike in the case of MMC. While the addition of ethylene glycol and ethanol showed a possibility of inducing slow cell proliferation, this effect should be negligible because the response to high concentration MMC was very quick.

The continuous cell density and death rate data are useful for analyzing the response. Although our experiments provided the limited cell death rate, complete cell death rate can be achieved by using dead cell staining, fluorescence imaging, and image processing to improve our system. This will be an important step in future studies.

4. Conclusion

The response to the change in resonant frequency for HepG2 cells varied according to the MMC concentration. For a low MMC concentration (<10 μmol L^{-1}), a delay in the response was observed; moreover, an additional decrease in the resonant frequency was noted for an extremely low MMC concentration (<1 μmol L^{-1}). The main morphological response to MMC was the increase in resonant frequency. The modeling curves fitted well with CLND curve for low MMC concentrations. However, a rapid response was noted for high MMC concentrations (>20 μmol L^{-1}), and the curve fitted well with the first-order lag response. The first-order lag response indicates that the response occurred simultaneously for all cells. Cell response patterns for a wide range of MMC concentrations were analyzed using the modeling curves via the QCM system with a microscope. Thus, it appears that the combined QCM and microscope system is useful for numerically analyzing the cell response of adherent cells. The different response patterns suggested that different cell death processes occurred by mitomycin C. This suggests that the QCM system could be utilized to study cell death in adherent cells.

Author contribution statement

Hiroshi Muramatsu: Conceived and designed the experiments; Analyzed and interpreted the data; Contributed reagents, materials,

analysis tools or data; Wrote the paper.>

Masahiro Naka, Sae Ito, Maki Kawamura: Performed the experiments; Analyzed and interpreted the data.>

Funding statement

Prof. Hiroshi Muramatsu was supported by Japan Society for the Promotion of Science {JP21K05118}.

Declaration of AI-assisted technologies in the writing process

During the preparation of this work the authors partly used DeepL Write in order to improve readability. After using this tool, the authors reviewed and edited the content as needed and take full responsibility for the content of the publication.

Data availability statement

All the data generated in this manuscript can be supplied from the corresponding author with a reasonable request.

Declaration of competing interest

The authors declare the following financial interests/personal relationships which may be considered as potential competing interests:Hiroshi Muramatsu reports financial support was provided by Japan Society for the Promotion of Science.

Acknowledgment

This study was partly supported by KAKENHI (JP21K05118). The authors thank Prof. Takeshi Matsui and Prof. Tomoyasu Sugiyama for the useful discussion and Ms. Masumi Hyuga, Ms. Ayaka Ichinohe, Mr. Long Hao, and Mr. Hibiki Yamaguchi for the technical assistance. The authors would like to thank Enago (www.enago.jp) for the English language review.

Appendix A. Supplementary data

Supplementary data to this article can be found online at https://doi.org/10.1016/j.heliyon.2023.e20047.

Abbreviations

CLND	cumulative log-normal distribution
CMOS	complementary metal oxide semiconductor
F–R	resonant frequency and resistance
ITO	indium-doped tin oxide
LED	light-emitting diode
MMC	mitomycin C
PC	personal computer
PLL:	poly-L-lysine
QCM	quartz crystal microbalance
USB:	universal serial bus

References

[1] G. Sauerbrey, Verwendung von Schwingquarzen zur Wägung dünner Schichten und zur Mikrowägung, Z. Physik 155 (1959) 206–222.
[2] K.K. Knazawa, J.G. GrdonII, The oscillation frequency of a quartz resonator in contact with a liquid, Anal. Chim. Acta 175 (1985) 99–105.
[3] H. Muramatsu, E. Tamiya, I. Karube, Computation of equivalent circuit parameters of quartz crystal in contact with liquids and study of liquid properties, Anal. Chem. 60 (1988) 2142–2146.
[4] S. Kurosawa, E. Tawara, N. Kamo, Y. Kobatake, Oscillating frequency of piezoelectric quartz crystal in solutions, Anal. Chim. Acta 230 (1990) 41–49.
[5] H. Muramatsu, K. Kimura, Quartz crystal detector for microrheological study and its application to phase transition phenomena of Langmuir-blodgett films, Anal. Chem. 64 (1992) 2502–2507.
[6] H. Muramatsu, X. Ye, T. Ataka, Micro-rheology changes of nafion films with electrochemical mass-transports in hydroquinone solutions and in situ measurement using a quartz crystal analyzer, J.Electroanal.Chem. 347 (1993) 247–255.
[7] S.M. Chang, J.M. Kim, H. Muramatsu, T. Ataka, C.S. Ha, Y.S. Kwon, Analysis of the phase change phenomena of PMMA and PVAC blends using quartz crystal analyzer (Q.C.A.), Mol.Cryst.Liq.Cryst. 280 (1996) 301–306.
[8] M. Rodahl, F. Höök, B. Kasemo, QCM operation in liquids: an explanation of measured variations in frequency and Q factor with liquid conductivity, Anal. Chem. 68 (1996) 2219–2227.
[9] J. Redepenning, T.K. Schlesinger, E.J. Mechalke, D.A. Puleo, R. Bizios, Osteoblast attachment monitored with a quartz crystal microbalance, Anal. Chem. 65 (23) (1993) 3378–3381.

[10] D.M. Gryte, M.D. Ward, W.S. Hu, Real-time measurement of anchorage-dependent cell adhesion using a quartz crystal microbalance, Biotechnol. Prog. 9 (1) (1993) 105–108.
[11] J. Wegener, A. Janshoff, H.J. Galla, Cell adhesion monitoring using a quartz crystal microbalance comparative analysis of different mammalian cell lines, Eur. Biophys. J. 28 (1998) 26–37.
[12] K.A. Marx, T. Zhou, A. Montrone, H. Schulze, S.J. Braunhut, A quartz crystal microbalance cell biosensor: detection of microtubule alterations in living cells at nM nocodazole concentrations, Biosens. Bioelectron. 16 (2001) 773–782.
[13] H. Muramatsu, S. Ito, A.H.A. Alsaleem, Monitoring and modeling of living cell responses in the attachment process and reaction to the antitumor reagent cisplatin studied by a quartz crystal microbalance combined with a microscope, Anal. Chem. 92 (2020) 7907–7914.
[14] J. Wegener, J. Seebach, A. Janshoff, H.J. Galla, Analysis of the composite response of shear wave resonators to the attachment of mammalian cells, Biophys. J. 78 (2000) 2821–2833.
[15] T. Zhou, K.A. Marx, A.H. Dewilde, D. McIntosh, S.J. Braunhut, Dynamic cell adhesion and viscoelastic signatures distinguish normal from malignant human mammary cells using quartz crystal microbalance, Anal. Biochem. 421 (2012) 164–171.
[16] D. Chronaki, D.I. Stratiotis, A. Tsortos, E. Anastasiadou, E. Gizeli, Screening between normal and cancer human thyroid cells through comparative adhesion studies using the Quartz Crystal Microbalance, Sens. Bio-Sens. Research 11 (2016) 99–106.
[17] M. Rodahl, F. Höök, C. Fredriksson, C.A. Keller, A. Krozer, P. Brzezinski, M. Voinova, B. Kasemo, Simultaneous frequency and dissipation factor QCM measurements of biomolecular adsorption and cell adhesion, Faraday Discuss 107 (1997) 229–246.
[18] C. Fredriksson, S. Khilman, B. Kasemo, D.M. Steel, In vitro real-time characterization of cell attachment and spreading, J. Materials Science, Materials in Medicine 9 (1998) 785–788.
[19] J. Li, C. Thielemann, U. Reuning D. Johannsmann, Monitoring of integrin-mediated adhesion of human ovarian cancer cells to model protein surfaces by quartz crystal resonators: evaluation in the impedance analysis mode, Biosens. Bioelectron. 20 (2005) 1333–1340.
[20] Z. Fohlerová, P. Skládal, J. Turánek, Adhesion of eukaryotic cell lines on the gold surface modified with extracellular matrix proteins monitored by the piezoelectric sensor, Biosens. Bioelectron. 22 (2007) 1896–1901.
[21] M.S. Lord, C. Modin, M. Foss, M. Duch, A. Simmons, F.S. Pedersen, F. Besenbacher, B.K. Milthorpe, Extracellular matrix remodelling during cell adhesion monitored by the quartz crystal microbalance, Biomaterials 29 (2008) 2581–2587.
[22] E. Watarai, R. Matsuno, T. Konno, K. Ishihara, M. Takai, QCM-D analysis of material–cell interactions targeting a single cell during initial cell attachment, Sens. Actuators, B 171–172 (2012) 1297–1302.
[23] P.J. Molino, Z. Yue, B. Zhang, A. Tibbens, X. Liu, R.M.I. Kapsa, M.J. Higgins, G.G. Wallace, Influence of biodopants on PEDOT biomaterial polymers: using QCM-D to characterize polymer interactions with proteins and living cells, Adv. Mater. Interfaces 1 (2014), 1300122.
[24] W.L. Kao, H.Y. Chang, K.Y. Lin, Y.W. Lee, J.J. Shyue, Effect of surface potential on the adhesion behavior of NIH3T3 cells revealed by quartz crystal microbalance with dissipation monitoring (QCM-D), J. Phys. Chem. C 121 (2017) 533–541.
[25] H.W. Kang, N. Otani, H. Muramatsu, S.M. Chang, J.M. Kim, Investigation of the extracellular matrix effect for the QCM/CCD cell activity monitoring system, J. Nanoscience and Nanotechnology 18 (8) (2018) 5777–5784.
[26] M. Noiri, K. Kushiro, S. Togo, K. Sato, H.Y. Yoshikawa, M. Takai, Y. Teramura, Influence of cell adhesive molecules attached onto PEG-lipid-modified fluid surfaces on cell adhesion, Colloids Surf. B Biointerfaces 175 (2019) 375–383.
[27] A.H.A. Alsaleem, S. Ito, K. Naemura, H. Muramatsu, Comparison of cultured cell attachment on a temperature-responsive polymer, poly-L-lysine, and collagen using modeling curves and a thermal-controlled quartz crystal microbalance, J. Biol. Phys. 47 (2021) 117–129.
[28] T. Zhou, K.A. Marx, M. Warren, H. Schulze, S.J. Braunhut, The quartz crystal microbalance as a continuous monitoring tool for the study of endothelial cell surface attachment and growth, Biotechnol. Prog. 16 (2000) 268–277.
[29] K.A. Marx, T. Zhou, A. Montrone, D. McIntosh, Quartz crystal microbalance biosensor study of endothelial cells and their extracellular matrix following cell removal: evidence for transient cellular stress and viscoelastic changes during detachment and the elastic behavior of the pure matrix, Anal. Biochem. 343 (2005) 23–34.
[30] H.W. Kang, K. Ida, Y. Yamamoto, H. Muramatsu, Monitoring of morphology and physical properties of cultured cells using a micro camera and a quartz crystal with transparent indium tin oxide electrodes after injections of glutaraldehyde and trypsin, Anal. Chim. Acta 624 (2008) 154–161.
[31] J.Y. Chen, L.S. Penn, J. Xi, Quartz crystal microbalance: sensing cell-substrate adhesion and beyond, Biosens. Bioelectron. 99 (2018) 593–602.
[32] V.N. Iyer, W. Szybalski, Molecular mechanism of mitomycin action: linking of complementary DNA strands, BIOLOGICAL SCIENCES 50 (2) (1963) 355–362.
[33] H. Ohara, T. Terasima, Lethal effect of mitomycin-C on cultured mammalian cells, Gann 63 (1972) 317–327.
[34] B.H. Xu, V. Gupta, S.V. Singh, Mechanism of differential sensitivity of human bladder cancer cells to mitomycin C and its analogue, Br. J. Cancer 69 (1994) 242–246.
[35] M. Tomasz, Y. Palom, The mitomycin bioreductive antitumor agents: cross-linking and alkylation of DNA as the molecular basis of their activity, Pharmacol. Ther. 76 (1997) 73–87.
[36] A. Franchittof, P. Pichierri, P. Mosesso, F. Palitti, Caffeine effect on the mitotic delay induced by G2 treatment with UVC or mitomycin C, Mutagenesis 13 (5) (1998) 499–505.
[37] U. Schraermeyer, M. Diestelhorst, A. Bieker, M. Theisohn, H. Mietz, C. Ustundag, G. Joseph, G.K. Krieglstein, Morphologic proof of the toxicity of mitomycin C on the ciliary body in relation to different application methods, Graefes Arch. Clin. Exp. Ophthalmol. 237 (1999) 593–600.
[38] S.G. Kang, H. Chung, Y.D. Yoo, J.G. Lee, Y.I. Choi, Y.S. Yu, Mechanism of growth inhibitory effect of Mitomycin-C on cultured human retinal pigment epithelial cells: apoptosis and cell cycle arrest, Curr. Eye Res. 22 (3) (2001) 174–181.
[39] T.I. Kim, H. Tchah, S.A. Lee, K.G. Sung, B.J. Cho, M.S. Kook, Apoptosis in keratocytes caused by mitomycin C, Invest. Ophthalmol. Vis. Sci. 44 (2003) 1912–1917.
[40] A. Nieto, C.M. Cabrera, P. Catalina, F. Cobo, A. Barnie, J.L. Cortés, A. Barroso del Jesus, R. Montes, A. Concha, Effect of mitomycin-C on human foreskin fibroblasts used as feeders in human embryonic stem cells: immunocytochemistry MIB1 score and DNA ploidy and apoptosis evaluated by flow cytometry, Cell Biol. Int. 31 (2007) 269–278.
[41] Y. Cho, M. Ogawa, M. Hirota, Y. Oshima, Effects of mitomycin C and colchicine on toxin production and cell cycle regulation in the dinoflagellate Alexandrium tamarense, Harmful Algae 10 (3) (2011) 235–244.
[42] T. Nakayama, N. Nozawa, C. Kawada, S. Yamamoto, T. Ishii, M. Ishizuka, T. Namikawa, S. Ogura, K. Hanazaki, K. Inoue, T. Karashima, Mitomycin C-induced cell cycle arrest enhances 5-aminolevulinic acid-based photodynamic therapy for bladder cancer, Photodiagnosis Photodyn. Ther. 31 (2020), 101893. Table S1.